NeuroImage 184 (2019) 214–226

Contents lists available at ScienceDirect

NeuroImage

journal homepage: www.elsevier.com/locate/neuroimage

Data-driven tensor independent component analysis for model-based connectivity neurofeedback

Yury Koush [a,*], Nemanja Masala [b], Frank Scharnowski [c,d,e,g], Dimitri Van De Ville [b,f]

[a] Department of Radiology and Biomedical Imaging, Magnetic Resonance Research Center (MRRC), Yale University, 300 Cedar Street, New Haven, CT, 06519, USA
[b] Institute of Bioengineering, Ecole Polytechnique Fédérale de Lausanne (EPFL), Campus Biotech, Chemin des Mines 9, 1202, Geneva, Switzerland
[c] Department of Psychiatry, Psychotherapy and Psychosomatics, Psychiatric Hospital, University of Zürich, Lenggstrasse 31, 8032, Zürich, Switzerland
[d] Neuroscience Center Zürich, University of Zürich and Swiss Federal Institute of Technology, Winterthurerstr. 190, 8057, Zürich, Switzerland
[e] Zürich Center for Integrative Human Physiology (ZIHP), University of Zürich, Winterthurerstr. 190, 8057, Zürich, Switzerland
[f] Department of Radiology and Medical Informatics, University of Geneva, Campus Biotech, Chemin des Mines 9, 1202, Geneva, Switzerland
[g] Department of Basic Psychological Research and Research Methods, Faculty of Psychology, University of Vienna, Liebiggasse 5, 1010, Vienna, Austria

ARTICLE INFO

Keywords:
Neurofeedback
Real-time fMRI
Visual-spatial attention
Data-driven
Model-based
Tensor independent component analysis
Dynamic causal modeling
Activation
Deactivation
Recovery processes

ABSTRACT

Neurofeedback based on real-time functional MRI is an emerging technique to train voluntary control over brain activity in healthy and disease states. Recent developments even allow for training of brain networks using connectivity feedback based on dynamic causal modeling (DCM). DCM is an influential hypothesis-driven approach that requires prior knowledge about the target brain network dynamics and the modulatory influences. Data-driven approaches, such as tensor independent component analysis (ICA), can reveal spatiotemporal patterns of brain activity without prior assumptions. Tensor ICA allows flexible data decomposition and extraction of components consisting of spatial maps, time-series, and session/subject-specific weights, which can be used to characterize individual neurofeedback regulation per regulation trial, run, or session. In this study, we aimed to better understand the spatiotemporal brain patterns involved and affected by model-based feedback regulation using data-driven tensor ICA. We found that task-specific spatiotemporal brain patterns obtained using tensor ICA were highly consistent with model-based feedback estimates. However, we found that the DCM approach captured specific network interdependencies that went beyond what could be detected with either general linear model (GLM) or ICA approaches. We also found that neurofeedback-guided regulation resulted in activity changes that were characteristic of the mental strategies used to control the feedback signal, and that these activity changes were not limited to periods of active self-regulation, but were also evident in distinct gradual recovery processes during subsequent rest periods. Complementary data-driven and model-based approaches could aid in interpretation of the neurofeedback data when applied post-hoc, and in the definition of the target brain area/pattern/network/model prior to the neurofeedback training study when applied to the pilot data. Systematically investigating the triad of mental effort, spatiotemporal brain network changes, and activity and recovery processes might lead to a better understanding of how learning with neurofeedback is accomplished, and how such learning can cause plastic brain changes along with specific behavioral effects.

1. Introduction

Neurofeedback based on functional magnetic resonance imaging (fMRI) is an emerging technique that allows training of voluntary control of brain activity and connectivity, and has been shown to lead to behavioral effects that are specific to the functional role of the targeted brain areas and networks (Sitaram et al., 2017). Growing scientific evidence indicates that most mental functions, and neurological and psychiatric disorders, are associated with brain network abnormalities assessed in terms of the various connectivity and network estimates (Bassett and Sporns, 2017; Braun et al., 2018). Similarly, neurofeedback research, which began from training the average activity level in a single region of interest (ROI) (deCharms, 2008; Sulzer et al., 2013), has advanced to training the behaviorally and therapeutically relevant functional activity patterns (Amano et al., 2016; deBettencourt et al., 2015; LaConte, 2011; LaConte et al., 2007; Shibata et al., 2011), and

* Corresponding author. Magnetic Resonance Research Center (MRRC), Yale University, 300 Cedar Street, New Haven, CT, 06519, USA.
E-mail address: yury.koush@yale.edu (Y. Koush).

https://doi.org/10.1016/j.neuroimage.2018.08.067
Received 20 April 2018; Received in revised form 21 July 2018; Accepted 28 August 2018
Available online 31 August 2018
1053-8119/© 2018 Elsevier Inc. All rights reserved.

connectivity and network estimates (Kajal et al., 2017; Kim et al., 2015; Koush et al., 2013, 2015; Liew et al., 2016; Megumi et al., 2015; Ramot et al., 2017; Yamashita et al., 2017; Zilverstand et al., 2014). Currently, the approaches for estimating connectivity for neurofeedback training can be separated into functional-connectivity estimates based on Pearson's correlation (Kajal et al., 2017; Kim et al., 2015; Liew et al., 2016; Megumi et al., 2015; Ramot et al., 2017; Yamashita et al., 2017; Zilverstand et al., 2014), and effective-connectivity estimates based on dynamic causal modeling (DCM) of the brain networks (Koush et al., 2013, 2015) given generic classification (Friston, 2011). Thus, the majority of the neurofeedback studies are based on hypothesis-driven processing methods typically used for the definition of the target brain areas/patterns/networks, feedback estimation in real-time, and post-hoc data analysis of the neurofeedback runs and sessions. In addition, independent component analysis (ICA) has been proposed to investigate fMRI data in real-time by providing data-driven activation maps using the sliding-window approach (Esposito et al., 2003; Soldati et al., 2013). Notably, ICA is part of the family of subspace decomposition methods, such as classical principal components analysis (PCA (Friston et al., 1999; Worsley et al., 1997)), and non-negative matrix factorization (Hoyer, 2004; Lohmann et al., 2007), which represent the data as a sum of separable components. The criterion of choice for ICA is a proxy for statistical independence applied to the spatial domain. When applied to task fMRI, ICA leads to components with brain activity maps similar to those of the conventional general linear model (GLM) approach, yet it also allows for the discovery of additional 'trends' in the data and, thus, extends interpretation of the fMRI data by capturing task- and rest-(un) related components (Beckmann, 2012; Kelly et al., 2010). The tensor extension of ICA, tensor ICA, allows data-driven multi-subject and multi-session analysis by representing the fMRI data in terms of their spatial, temporal, and subject-dependent variations (Beckmann and Smith, 2005), whose potential for neurofeedback studies has yet to be revealed. In particular, tensor ICA explains data using a tensor structure (time × space × session/subjects), such that a component with a specific spatial map and time-series is weighted for each session/subject. The latter weights could then be used to explore the model-based neurofeedback post-hoc, and for an effective complementary data-driven and model-based definition of the target brain areas/patterns/networks prior to the whole-length neurofeedback studies. In addition, tensor ICA is more constrained than conventional ICA, since it requires space and time to be consistent across subjects; conventional ICA has only two dimensions space × time, and concatenates subjects along the temporal dimension.

It has been shown that neurofeedback estimates based on DCM can be implemented and validated using an alternating neurofeedback-guided paradigm (Koush et al., 2013). In particular, the connectivity-based differential feedback presented in Koush et al. (2013) was congruent with the conventional alternating visual-spatial attention task (Bressler et al., 2008a; Greenberg et al., 2010; Hopfinger et al., 2000); for example, during neurofeedback regulation trials with covert shifts of visual-spatial attention to the left, the network model that represented attention to the left was dominant compared to the model that represented attention to the right, and vice versa during attention to the right neurofeedback regulation trials. Such a validated effective-connectivity estimate has been also successfully applied to train voluntary control over emotion regulation networks (Koush et al., 2015). Notably, DCM is a hypothesis-driven approach that requires defining the neural network underlying a specific functional neuroimaging experiment in terms of the network nodes (ROIs), connections between these nodes, external inputs to the network, and context-dependent manipulations of the network (Friston et al., 2003).

We hypothesized that tensor ICA could be applied to connectivity-based neurofeedback experiments on a trial-by-trial basis, with the specific constraint that the time-series of the tensor ICA components are weighted by the neurofeedback trial loadings. We investigated whether tensor ICA and DCM could be qualitatively linked, and provide complementary data-driven and model-based insights into the neurofeedback-guided dataset. In addition, we aimed to shed light on the potential dynamic recovery process from induced (de)activation, which might take place during the relatively long rest epochs (1 min) following neurofeedback-guided alternating visual-spatial attention regulation. This was accomplished by analyzing data from a previously published study (Koush et al., 2013), which possesses (1) a well-known alternating visual-spatial attention paradigm, (2) distinct network models and differential feedback values congruent with the alternating regulation task, and (3) rest epochs at the end of each neurofeedback trial. Complementary data-driven and model-based approaches could aid in interpretation of the neurofeedback data when applied post-hoc, and in the definition of the target brain areas/patterns/networks/models when applied to the pilot data. In addition, task- and rest-related epochs of the complex neurofeedback experimental paradigms could be jointly characterized using the data-driven approach, and linked to the model-based feedback estimates. Establishing a link between model-based and data-driven approaches for neurofeedback research together with a systematic investigation of the triad of mental effort, spatiotemporal brain network changes, and activity and recovery processes, might lead to a better understanding of how neurofeedback regulation is accomplished.

2. Methods

The analyses of our study were based on data from a previously published study, which was designed as a proof-of-concept experiment to validate the novel DCM-based estimate for connectivity feedback (Koush et al., 2013). In this experiment, we tested the ability of participants to voluntarily control the differential connectivity-based feedback signal by covertly shifting their visual–spatial attention to the left or to the right visual fields. The connectivity between visual and parietal areas is known to be modulated by visual-spatial attention (Blankenburg et al., 2010; Bressler et al., 2008b; Greenberg et al., 2010), which was a well suited paradigm for our proof-of-concept experiment. Thus, the modulation of the feedback signal was implicated in the alternating increase of connectivity between the right/left visual and parietal cortices during contralateral shifts of attention to the left/right, respectively. This connectivity feedback signal was based on a comparison of two alternative DCM models, which modelled visual-spatial attention to the left or to the right, and encompassed bilateral visual and parietal areas (see 'Stimuli and experimental design' and 'Differential neurofeedback signal' sections). For the current study, we briefly describe the experimental settings. Further experimental details and thorough analyses of the DCM-based connectivity estimate can be found in the original publication (Koush et al., 2013).

2.1. Participants

Imaging data was acquired from fourteen participants (5 male, 9 female, age 27.2 ± 5.2 years) who were naïve to neurofeedback experiments. All participants performed visual perception and visual-spatial attention functional localizer runs (i.e., without neurofeedback). Seven participants performed only the functional localizer runs, whose data were used to optimize the DCM feedback estimates (Koush et al., 2013). The seven other participants performed the complete neurofeedback experiment (3 male, 4 female, age 27.7 ± 3.3 years), including the functional localizer runs and the neurofeedback runs. The participants gave written informed consent to participate in the experiment, which was approved by the local ethics committee, and had normal or corrected-to-normal vision without prior history of neurological or psychiatric diseases. Written instructions provided to the participants before the experiment described that they would perform a single visual perception run, two covert visual-spatial attention functional localizer runs (i.e., without neurofeedback), and three covert visual-spatial attention regulation runs (i.e., with neurofeedback). The instructions included an explanation of the experimental conditions. For

neurofeedback regulation runs, instructions also included an explanation of the neurofeedback display, and the fact that they would receive neurofeedback information about their regulation success. The strategy for controlling connectivity between brain areas that was recommended to participants was shifting of visual-spatial attention; however, it was emphasized that they should find an individual strategy that worked best. Furthermore, they were instructed to breathe steadily, and to remain as still as possible. After the experiment, participants were asked to fill in the neurofeedback regulation questionnaire and report the applied regulation strategies. Participants were paid 25 CHF per hour for their participation, and received an additional reward of 1 CHF for each successful neurofeedback trial.

2.2. MRI data acquisition

The experiments were performed at the Brain and Behavior Laboratory (University of Geneva) on a 3T MRI scanner (Trio Tim, Siemens Medical Solutions, Germany). Functional images were acquired with a single-shot gradient-echo T2*-weighted EPI sequence with 640 and 1315 scans (32 channel receive head coil, TR = 1000 ms, volume size = 64 × 64 × 16, voxel size = 3 mm^3 isotropic, flip angle $\alpha = 77^\circ$, bw = 2.23 kHz/pixel, TE = 30 ms). For each participant, we acquired a T1-weighted structural image (3D MPRAGE, voxel size = 1 mm^3 isotropic, flip angle $\alpha = 9^\circ$, TR = 1900 ms, TI = 900 ms, TE = 2.27 ms). We monitored eye movements with an infrared eye-tracking system (ASL 450, 60 Hz sampling rate, LRO System). In addition, heart rate and respiration were continuously monitored throughout the experiment with a modular data acquisition system (MP150, 1kHz sampling rate, BIOPAC Systems Inc.). Heart rate was measured using a pulse oximetry sensor, and respiration was measured using an elastic belt around the participant's chest. Visual stimuli and instructions were displayed on a rectangular projection screen at the rear of the scanner bore with a mirror positioned within the head-coil.

2.3. Stimuli and experimental design

For each of the fourteen participants, we first ran a single fMRI session that consisted of three successive functional localizer runs: a visual perception run, and two runs of visual-spatial attention to the left or to the right, respectively. Each of the three runs consisted of 11 baseline blocks interleaved with 10 blocks of task (10 s block length). For the visual perception task, we used symmetrical flickering checkerboards presented simultaneously in the left and right visual field to delineate the early visual cortex. Flickering checkerboards were projected onto the middle horizontal axis of the screen with an eccentricity of 5° visual angle (diameter of 5° visual angle, 100% contrast, 8 Hz contrast reversal). For the visual-spatial attention runs, we instructed participants to shift their visual-spatial attention covertly (i.e., without moving their eyes) to the left or to the right as indicated by changes in the fixation point. The target location for shifting attention was illustrated by low-contrast dashed circles that were of the same diameter and presented at the same location as the visual checkerboards. Throughout the visual perception run and the visual-spatial attention runs, the participants were asked to fixate on the central fixation point. The total duration of the visual perception and attention runs was 10.3 min.

Seven out of the fourteen participants also performed the neurofeedback regulation runs. The functional localizer runs were used to delineate individual left and right early visual cortex (VC), and the left and right superior parietal lobule (SPL) ROIs. These ROIs were used to estimate the connectivity-based feedback signal individually for each of three neurofeedback regulation runs performed within the same day. Each of the subsequent neurofeedback regulation runs was set up as four attention to the left (aL) neurofeedback trials alternating with four attention to the right (aR) trials. Each of the neurofeedback trials consisted of five 10s baseline blocks (fixation condition) interleaved with four 10s blocks of the corresponding regulation (aL or aR condition) followed by a 60s rest epoch and 5s neurofeedback display (Fig. 1A).

During the aL and aR conditions, participants were asked to control the feedback signal by covertly shifting their attention to the left or to the right target dashed circles, respectively. The covert shifts of attention were indicated by fixation dot changes: the brighter half of the fixation circle pointed to the side of the prescribed attention. During the fixation condition, participants were asked to fixate and count backwards to avoid mind-wandering, which was indicated by the plain low-contrast fixation dot. During neurofeedback trials, bilateral dashed circles and the pointed fixation circle were always presented, and no other visual stimuli were provided. During the rest epochs, participants were asked to close their eyes, and the screen was set to black. After each rest epoch, 3 auditory beeps and 3 visual flashes indicated to the participant that the feedback and reward values were displayed on the screen. The feedback signal display indicated the feedback trial (the word “UP” in red for aL trials, or the word “DOWN” in blue for aR trials), the feedback signal in terms of the rounded logarithmic Bayes factor value in brackets (positive for successful aL trials and negative for successful aR trials), and the total reward that had been earned up to the present trial. The duration of the neurofeedback run was 21.8 min.

2.4. Differential neurofeedback signal

The two models that we compared represented covert shifts of visual-spatial attention to the left or right visual field, and consisted of 4 ROIs, being the interconnected left visual and parietal cortices and the interconnected right visual and parietal cortices (Fig. 1B). The difference between the models was the external and the modulatory inputs of attention, which should be stronger on the right SPL and on the connectivity between the right VC and the right SPL when attention is covertly shifted to the left visual field (M_{aL}), and stronger on the left SPL and on the connectivity between left VC and the left SPL when attention is covertly shifted to the right visual field (M_{aR}). The model choice was based on the suggested modulation of the connectivity between visual and parietal areas by visual-spatial attention (Blankenburg et al., 2010; Bressler et al., 2008b; Greenberg et al., 2010; Kelley et al., 2008; Yantis et al., 2002) and performed near real-time DCM optimization analyses (Koush et al., 2013).

Real-time data preprocessing encompassed online motion correction and extraction of the time-series as ROI-specific averages, which was followed by time-series demeaning, high- and low-pass filtering, and despiking (Koush et al., 2012). The trial-based feedback signal was estimated as the result of Bayesian model comparison of the two alternative models in terms of the logarithmic Bayes factor given the four preprocessed time-series. Successful control over the feedback signal was indicated by positive and negative target feedback values. For attention to the left trials, a positive logarithmic Bayes factor (BF) indicated the dominance of the target M_{aL} model. A negative logarithmic BF indicated the dominance of the target M_{aR} model. The connectivity-based feedback signal was estimated by adapting DCM10 as implemented in SPM8 (Wellcome Trust Centre for Neuroimaging, UK) (Friston et al., 2003). Further details about data processing and the connectivity-based neurofeedback signal can be found elsewhere (Koush et al., 2013, 2015). Notably, an open-source software framework *OpenNFT* (opennft.org) (Koush et al., 2017a) provides an improved implementation of the trial-based DCM estimation scheme; namely, DCM models can be computed in parallel, and an extension is provided to integrate the linear trend and head motion residuals directly into the DCM model estimation. In addition, an exemplary dataset (github.com/OpenNFT) (Koush et al., 2017b) and provided supplementary routines allow testing of the DCM estimation schemes before implementing them in OpenNFT.

2.5. Data analyses

In addition to the DCM analyses, whole-brain GLM analysis was performed to support the interpretation of the DCM and tensor ICA

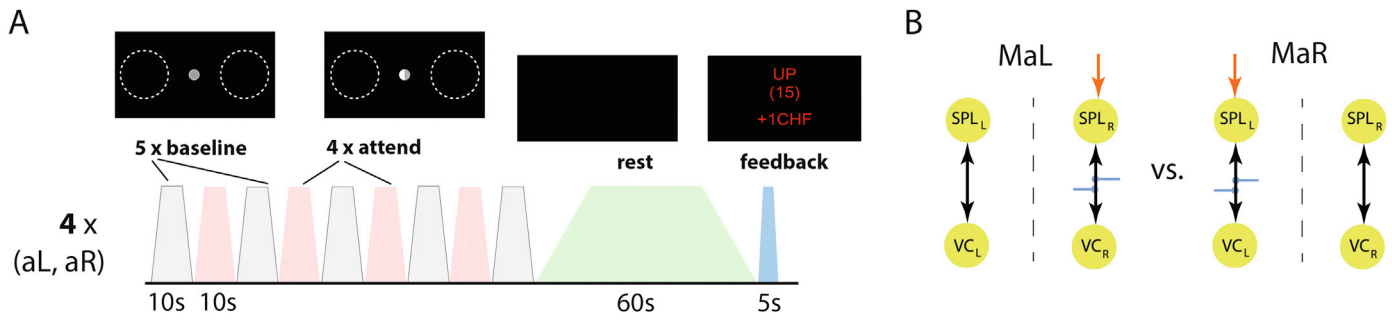

Fig. 1. Neurofeedback trial. (A) Each neurofeedback run consisted of 8 alternating trials of covert visual-spatial attention to the left (aL) or to the right (aR). Each trial consisted of four 10s neurofeedback regulation blocks (attend) interleaved with five 10s baseline blocks (baseline) followed by a 60s rest epoch and a 5s presentation of the feedback display. During the regulation blocks, the brighter half of the fixation circle pointed to the side of the prescribed attention. The screenshots illustrate the bilateral dashed circles and low-contrast plain and pointed fixation dots for the baseline and aL blocks, respectively. (B) In the models of attention to the left (M_{aL}), input entered the network through the right superior parietal lobe (SPL_R) and affected the connection between the SPL_R and the right visual cortex (VC_R); in the model of attention to the right (M_{aR}), input entered the network through the SPL_L and affected the connection between the SPL_L and the VC_L (for details, see (Koush et al., 2013)).

analyses. The first 10 EPI volumes of each run were discarded to account for T1 saturation effects. The remaining images were spatially realigned to the mean scan of each run, normalized to the standard MNI structural template using DARTEL (Ashburner, 2007), and smoothed with an isotropic Gaussian kernel with 8 mm full-width-at-half-maximum (FWHM).

For the subject-level analysis of the visual perception and visual-spatial attention functional runs, we specified GLMs with regressors for the three conditions (i.e., viewing, left attention, right attention) and fixation. For the subject-level analysis of the neurofeedback runs (Fig. 1A), we specified regressors for the two attention conditions (REG aL and aR, respectively), the two fixations with counting backwards (FIX aL and aR, respectively), the two rest epochs, and the neurofeedback display conditions.

To capture the gradual recovery of brain activity to baseline, the 60s rest epochs were split into three equal parts of 20s that were modelled separately. Specific contrast weights were adopted for linear trend estimates of recovery; i.e., [-1 0 1] and [1 0 -1] for positive and negative trends, respectively. In addition, we specified temporal derivatives of all conditions and fixations and of covariates derived from head movement parameters and physiological measures (i.e., heart rate and respiration). The temporal derivatives were included in the model to account for potential hemodynamic response function (HRF) onset latencies that might have been modulated differently by the transition from regulation to fixation, from fixation to rest, and between the rest conditions (Van De Ville et al., 2012). The inclusion of temporal derivatives ensured that our findings would be specific to the gradual recovery process during the rest epoch, rather than to potential biases due to other transition processes. The regressors were modeled as boxcar functions convolved with the canonical hemodynamic response function (HRF) as implemented in SPM12.

For the whole-brain group-level analysis, we performed 2-way ANOVAs with the fixed factor 'condition' and random factor 'subject'. For 'conditions' in visual perception and visual-spatial attention runs, we included viewing, left attention, right attention, fixations, and covariates for the participants' age and gender. For 'conditions' in the neurofeedback runs, we included left/right attention regulation, fixations with counting, and the three rest epochs (i.e., the three 20s segments comprising the 60s rest epochs). For the three consecutive neurofeedback runs, the fixed effect model was applied. For covariates, we included the participant's age, gender, and neurofeedback run number. Notably, including the run number ensured that improved performance across neurofeedback trials did not affect the results, i.e. as it has been noted above, unveiling the learning effect was not a goal of the study. Instead, we looked into the congruent aL vs. aR regulation and DCM-based feedback values. We used t-statistics to estimate positive and negative contrasts of interest. Group-level statistical maps were corrected for multiple comparisons using family-wise error correction (FWE, $p < .05$). Anatomical labels were derived from the Anatomy toolbox (Eickhoff et al., 2005).

2.6. ROI definitions and time-series extraction for rest epoch analyses

ROIs for the offline analyses were defined as spheres of 8 mm radius around peaks that showed a significant gradual recovery across rest epochs. For each ROI, we calculated the average contrast estimates of deactivation (beta values) during the neurofeedback regulation and the slope of linear recovery (Fisher-transformed rho values) during rest epochs. We then performed a correlation analysis between the deactivation and recovery rho values using Spearman correlation. All probabilities were FDR-corrected for multiple comparisons ($q < .05$).

2.7. Revisited dynamic causal modeling (DCM) analysis of neurofeedback regulation trials

For comparison, real-time signal processing and DCM analysis applied during the neurofeedback runs (Koush et al., 2013) were revisited based on the newly preprocessed data (i.e., realigned, transformed into the MNI space, and smoothed). Functional localizer data (also transformed into the MNI space) were used to re-define individual ROIs, similarly to what was done during the neurofeedback regulation session. Subsequently, the four time-series were extracted from the neurofeedback trials as ROI-specific averages, followed by demeaning and detrending using the GLM with constant and linear trend regressors. Similar low-pass filtering and despiking were applied based on the Kalman filter (Koush et al., 2012, 2017a). Using the newly preprocessed time-series, the trial-based feedback signal was estimated by Bayesian model comparison of the same M_{aL} and M_{aR} model alternatives (Fig. 1B) in terms of the logarithmic Bayes factor. In order to re-confirm that voluntary control over the feedback signal favored MaL (Pe_{MaL}) or MaR (Pe_{MaR}) for the attention to the left (aL) or to the right (aR) conditions, respectively, we estimated the quantified model exceedance probabilities (Pe (Stephan et al., 2009),) as implemented in the random effect Bayesian model selection (RFX BMS, DCM10). To confirm that the newly estimated logarithmic Bayes factors were consistent with regulation during aL and aR neurofeedback trials, we estimated the non-parametric sign test statistics (one-tailed, median > 0). Z-statistics was used to approximate the p-values of the non-parametric sign test. For a complete DCM analysis of the neurofeedback runs and a comparison analysis between functional localizer and neurofeedback runs, refer to the original manuscript (Koush et al., 2013).

2.8. Tensor independent component analysis (ICA)

In order to link the DCM-based feedback estimates to data-driven spatio-temporal features and to test whether model-free methods could be used to facilitate the ROI selection procedures for DCM-based approaches in neurofeedback studies, we performed an exploratory tensor ICA (Beckmann, 2012; Beckmann and Smith, 2005) and subsequent correlation analysis. We split the preprocessed neurofeedback runs, which had been used for the whole-brain GLM analysis, into the eight neurofeedback trials that were demeaned, resulting in 84 aL and 84 aR demeaned trials (7 subjects, 3 neurofeedback runs, 4 aL/aR trials per run, 155 brain volumes per trial). Note that the runs were split so that the preceding 5 s feedback display blocks appeared at the beginning of the trials to highlight the brain response to the feedback evaluation. These neurofeedback trials were used as 'session loadings' for tensor ICA, and will be called 'trial loadings' throughout the manuscript. Tensor ICA decomposes the preprocessed data into the spatial maps, time-series, and subject-specific trial modes by optimizing for non-Gaussian spatial source distributions. It was carried out as implemented in the Multivariate Exploratory Linear Decomposition into Independent Components (MELODIC v3.15) package of FSL (fsl.fmrib.ox.ac.uk/fsl). Pooled neurofeedback trials were preprocessed (i.e., masking of non-brain voxels, voxel-wise demeaning, and normalization of the voxel-wise variance as implemented in MELODIC). FSL then whitens and reduces the dimensionality of the data using principal component analysis as an internal preprocessing step, before the ICA criterion is optimized. Independent component (IC) maps were estimated, Z-scored by dividing by the standard deviation of the residual noise, and thresholded (posterior probability $p > .5$) by fitting a mixture model to the histogram of intensity values (Beckmann, 2012; Beckmann and Smith, 2004).

The selection of the optimal number of the components (i.e., model order, number of ICs) remains a challenge for techniques such as ICA and PCA. We first defined the #ICs based on the automatic choice of dimensionality as implemented in FSL (Beckmann et al., 2001; Minka, 2000). However, this method is known to overestimate the number of components with many fragmented maps that make interpretation difficult. Therefore, and because we have an experimental paradigm that we proposed to relate to a few 'dominant' components, we opted for a small number of components. Specifically, we checked the automatically defined #ICs = 24 and the range from 6 to 12 #ICs. For each #IC, we performed the same correlational analysis.

Using Spearman two-tailed correlation, tensor ICA trial loadings were correlated with the logarithmic model evidences of the corresponding target DCM models, i.e., for the M_{aL} model during aL and the M_{aR} model during aR regulation conditions, respectively (168 trial loadings and logarithmic model evidences, 84 of aL and 84 of aR trials). To avoid inter-subject variability bias, logarithmic model evidences and trial loadings were demeaned. P-values were corrected for multiple comparisons using family-wise error correction (FWE, $p < .05$). In addition, we performed the same correlation analysis for the estimated logarithmic Bayes factors.

To demonstrate the spatial consistency of the linked ICA and DCM results with the initial ROI selections for the neurofeedback runs based on the functional localizers, we compared group GLM contrast maps (thresholded at $p < .01$ unc.) and derived ICs that were significantly correlated with logarithmic model evidences. For this comparison, we used the Pearson cross-correlation algorithm as implemented in FSL (*fslcc*) given a Pearson rho > 0.25 threshold (Smith et al., 2009).

2.9. Debriefing of participants

After each scanning session, participants were asked to fill in a written questionnaire and describe the strategies that they used to control the feedback signal. We also asked them to rate, on a scale from 1 to 5, (a) how helpful the feedback was in finding this strategy (i.e., the feedback was not helpful vs. helpful), (b) how vivid their visual imagery was (i.e., visual imagery was not vivid vs. vivid), and (c) how often they used other sensory modalities (i.e., they used acoustic and somatosensory imagery often vs. not often). In addition, we asked participants to what extent successful self-regulation required them to concentrate (i.e., self-regulation required utmost concentration vs. no concentration), and how they rated the attentional demands (i.e., focused vs. absent-minded). Using Spearman one-tailed correlation, the scores from these psychometric measures were correlated with the degree to which participants were able to control their visual-spatial attention (i.e., neurofeedback success estimated in terms of the logarithmic Bayes factor averaged across neurofeedback trials (Koush et al., 2013)). All probabilities were FDR-corrected for multiple comparisons ($q < .05$).

3. Results

3.1. Brain activity associated with visual perception and shifting visual-spatial attention

We first identified brain areas that were modulated by viewing spatially localized flashing checkerboards and by covert shifts of visual-spatial attention to the left or to the right visual field. As expected, viewing the flickering checkerboard stimuli was associated with increased activity in the V1, V2, and ventral V3 cortices (Table 1, Fig. 2A). Covertly shifting visual-spatial attention to the left or to the right visual field (attention > fixation) was associated with increased activity in the left superior parietal lobule (SPL). We found no significant differences in brain activity when contrasting the aL and aR conditions.

Covert visual-spatial attention was associated with activity increases (attention, activation) in the SPL, intraparietal sulcus (IPS), and the supplementary motor area (SMA), and with decreases (attention, deactivation) in the middle cingulate cortex (MCC), inferior parietal lobule (IPL), precuneus, posterior cingulate cortex (PCC), primary and secondary sensorimotor cortices (S1 and SII), and the motor cortex (MC) (Table 1, Fig. 2B).

3.2. Brain activity associated with control over the neurofeedback signal

During neurofeedback regulation (REG > FIX), the bilateral SPL was activated more than during fixation (Table 2). Neurofeedback regulation was also associated with activation (i.e., positive REG contrast) in the SPL and ventral V3/V4, medial frontal gyrus (MFG) and IPS, as well as with deactivation (i.e., negative REG contrast) in the V1/V2/V3, lingual (LG), V5/MT, IPL, MCC/SMA, SII, precuneus/PCC, medial frontal cortex (FC) and dorsolateral prefrontal cortex (dlPFC) (Table 2, Fig. 3). Notably, voluntary control of the feedback signal was not related to horizontal and vertical eye-positions, which showed no difference between regulation and fixation blocks during the visual perception runs, the visual-spatial attention runs, or the neurofeedback runs (for details, see (Koush et al., 2013)).

In addition, contrasts aL > aR (Fig. 3B, Table 2) and aR > aL (Fig. 3C, Table 2) showed that visual cortices were differently involved in the attention tasks. For example, during attention to the left, the left ventral V3 was activated more than during attention to the right, and during attention to the right, the left anterior V3 was deactivated more than during attention to the left. These areas do not coincide with the DCM ROIs selected using the visual functional localizer (Fig. 2).

3.3. Linking DCM and tensor ICA for neurofeedback-guided regulation

The feedback signal in terms of the re-estimated logarithmic Bayes factor was significantly greater than zero (one-tailed sign test and z-statistics, sign = 99, z = 2.2, p = .01, negative aR feedback values were inverted), and the successful neurofeedback regulation was reflected by increased target model exceedance probabilities of model M_{aL} during aL ($Pe_{MaL} = 0.86$, $Pe_{MaR} = 0.14$) and model M_{aR} during aR ($Pe_{MaL} = 0.23$, $Pe_{MaR} = 0.77$) regulation conditions, respectively.

We found that our dataset provides consistent ICA decompositions

Table 1
Brain areas related to passive viewing and covert visual-spatial attention.

contrast	anatomical label		main peak MNI coordinates			Peak T-value	Peak p-value
			x	*y*	*z*		
viewing	V1/V2/V3v	L/R	−7/13	−95/-88	−5/-5	5.39/5.55	.009/.005
attention > fixation	SPL (7A/7P)	L	−11	−68	61	5.50	.006
attention (activation)	SPL (7A/7P)	L/R	−13/18	−68/-61	61/63	8.56/5.98	<.001/.001
	IPS	L/R	−36/31	−43/-40	36/43	6.02/5.64	.001/<.001
	SMA	L/R	−2/0	9/16	58/50	4.91/5.19	.042/.037
attention (deactivation)	MCC	L	−4	−23	63	5.97	.001
	IPL (PGa)	R	56	−58	34	5.85	.002
	Prec./PCC	R	5	−43	38	4.97	.035
	SII (PO)	L	−40	−29	9	5.77	.002
	S1	L	−61	−11	36	7.28	.022
	MC	L/R	−13/20	−36/-36	72/76	7.44/7.02	<.001/<.001
	MC/S1	R	36	−32	68	6.26	<.001

Reported are the main peaks that survived whole-brain FWE correction ($p < .05$). V1/V2/V3v – visual cortices, SPL(7A/7P) – superior parietal lobule, IPS – itraparietal sulcus, SMA – supplementary motor area, MCC – middle cingulate cortex, IPL(PG) – inferior parietal lobule (precentral gyrus), SII (PO) – secondary somatosensory cortex (parietal operculum), S1 – primary somatosensory cortex, MC – motor cortex, L – left, R – right, a – anterior, v – ventral.

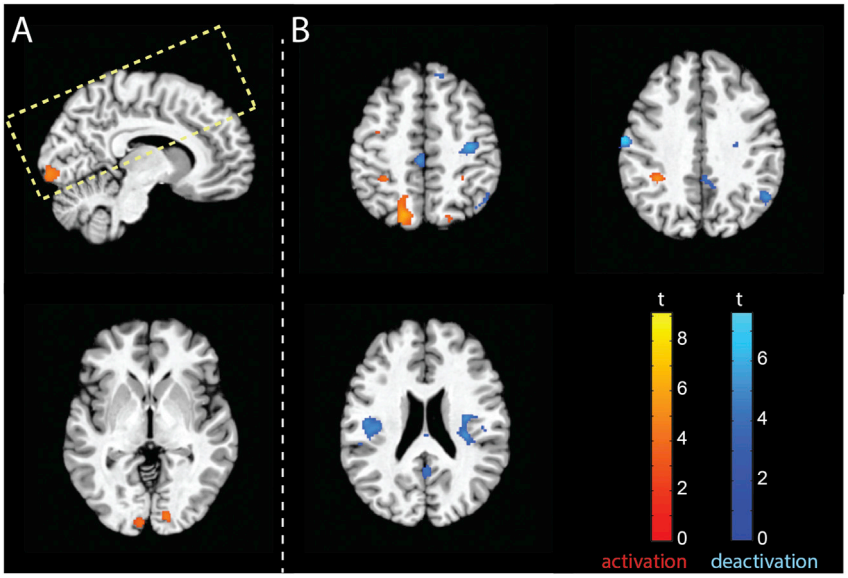

Fig. 2. Visual perception and covert visual-spatial attention. (A) Viewing localized bilateral flashing checkerboards was associated with increased activity in the visual cortex (Table 1, viewing). (B) Covert shifts of visual-spatial attention to the left or to the right were mainly associated with activity in the left but also the right SPL (Table 1). For illustration, the activation maps were thresholded ($p < .0001$ unc.). The yellow dashed rectangle denotes the acquired field of view.

and correlational analyses when automatically defining the subspace dimension as implemented in FSL (#ICs = 24: $rho_{IC17} = 0.27$, $p_{IC17} = 0.01$), and when varying across low subspace dimensions from 6 to 12 (Table S1). Because automatic definition of the #ICs provides many fragmented maps that are difficult to interpret, and because we have an experimental paradigm that we aimed to relate to a few representative components, we reported the results for #ICs = 10 in detail (Figs. 4 and S1).

Thus, preprocessed neurofeedback trials for tensor ICA were decomposed into a set of #ICs = 10 spatial maps and time-series. ICs eight to ten were visually identified as noise and removed from the subsequent analysis (Kelly et al., 2010). The first IC encompassed V1-V4, V5/MT, SPL, and IFG, anticorrelated with primary motor and premotor cortices, PCC, SII, and aIPL clusters (Fig. 4A). The second and fourth ICs encompassed V1/V2/LG medial visual cortices (Figs. 4A and S1A). Importantly, the third IC corresponded to the lateral V1/V2/V3v, matching the ones from the functional localizer (Fig. 2A). The fifth IC was similar to the first IC and, additionally, encompassed the SMA/MCC, PG, and IPS clusters (Fig. S1A). The sixth IC was similar to the fifth IC and, additionally, encompassed the medial FC and a large cluster spanning the PCC, part of the precuneus, and V1/V2 (Fig. S1A). The seventh IC encompassed SII, SI, and primary motor cortices (Fig. S1A).

All ICs showed neurofeedback regulation-dependent temporal dynamics (Fig. 4B, S1B). The first and third ICs showed strong recovery processes during the rest epoch, unlike the second and fourth ICs. Interestingly, the fifth, sixth, and seventh ICs did not show the amplitude rise associated with the feedback display block and closing the eyes at the beginning of the rest epoch. Note that the second and fourth ICs have very similar spatial and temporal modes; however, only the second IC survived FWE correction for multiple comparisons. We did not find differences between aL and aR trial loadings (two-tailed t-statistics, p-values>.5), which suggested that the ICs were expressed similarly in both conditions.

For each IC, 168 trial loadings, or weights, were estimated in the trial domain (84 of aL and 84 of aR trials). We found that demeaned logarithmic model evidences of target model M_{aL} during aL and target model M_{aR} during aR regulation conditions were correlated with the intra-subject trial loadings of the first three ICs (Fig. 4C, two-tailed

Table 2
Brain areas activated during neurofeedback runs.

contrast	anatomical label		main peak MNI coordinates			Peak t-value	Peak p-value
			x	y	z		
REG > FIX	SPL (7A/7P)	L/R	−18/18	−69/-66	54/60	5.19/5.16	.003/.004
REG (activation)	SPL (7A/7P)	L/R	−9/18	−72/-69	57/54	7.48/6.30	<.001/<.001
	V3v/V4v	L/R	−24/33	−93/-81	−15/-15	55/5.01	.001/.006
	MFG	R	45	3	57	4.65	.030
	IPS	L	−33	−42	48	4.57	.040
REG (deactivation)	V1/V2/V3	L/R	−9/9	−87/-84	24/18	9.90/11.06	<.001/<.001
	V1/V2/LG	L/R	−15/12	−60/-63	0/0	14.98/14.13	<.001/<.001
	V5/MT	R	45	−84	12	6.62	<.001
	IPL (PGa)	L/R	−60/57	−60/-54	27/36	6.08/7.46	<.001/<.001
	MCC/SMA	L/R	−9/9	−6/-15	45/45	5.57/5.63	.001/.001
	SII (PO)	L/R	−39/57	−36/-27	12/15	11.18/10.29	<.001/<.001
	Prec./PCC	R	−6/6	−45/-45	42/39	5.96/6.49	<.001/<.001
	medial FC	R	6	30	48	5.77	<.001
	dlPFC	R	48	30	39	5.63	.001
aL > aR	V3v/V4v	L	−27	−96	−12	6.70	<.001
aR > aL	V1/V2/V3	L	−18	−96	15	5.91	<.001

Reported are the main peak coordinates that survived whole-brain FWE correction ($p < .05$). REG – neurofeedback regulation, FIX – fixation with counting, SPL (7A/7P) – superior parietal lobule, V1-V5 – visual cortices, MFG – middle frontal gyrus, IPS – itraparietal sulcus, MT – middle temporal gyrus, LG – lingual gyrus, IPL(PG) – inferior parietal lobule (precentral gyrus), MCC/SMA – activity pattern spanning middle cingulate cortex and supplementary motor area, SII (PO) – secondary somatosensory cortex (parietal operculum), Prec./PCC – activity pattern spanning precuneus and posterior cingulate cortex, FC – frontal cortex, dlPFC – dorsolateral prefrontal cortex, L – left, R – right, a, v – anterior, ventral.

Table 3
Gradual recovery during rest epochs.

contrast	anatomical area		main peak MNI coordinates			Peak t-value	Peak p-value
			x	F-value	z		
recovery	V1/V2/V3v	L/R	−6/15	−81/-84	−6/-9	4.96/5.43	.009/.001
	V1/V2/LG	L	−9	−66	3	4.75	.021
	V3a	L/R	−15/15	−72/-84	24/27	4.82/5.05	.016/.006
	V5/MT	R	45	−66	9	4.87	.013
	MCC/SMA	L/R	−6/6	3/9	51/54	5.13/5.61	.001/.004
	PG	R	45	−3	51	4.89	.012
	Precuneus	R	3	−48	45	4.59	.037
	Thalamus	C	0	−9	9	4.89	.012
	dlPFC	L	−33	42	30	4.71	.024
conjunction (REG deactivation & recovery)	V1/V2/V3	R	−6/21	−81/-96	−6/6	4.82/5.48	.016/.001
	V1/V2/LG	L	−9	−66	3	4.75	.021
	V3a	L/R	−15/18	−72/-84	24/27	4.82/5.05	.016/.006
	V5/MT	R	42	−66	9	4.84	.014
	Precuneus	R	3	−48	45	4.59	.037

Reported are the main peak coordinates that survived whole-brain FWE correction ($p < .05$). REG – regulation, V1-V5 – visual cortices, MT – middle temporal gyrus, MCC/SMA – activity pattern spanning middle cingulate cortex and supplementary motor area, PG – precentral gyrus, dlPFC – dorsolateral prefrontal cortex, C – central, L – left, R – right, a, v – anterior, ventral.

Spearman correlation; first IC: rho = 0.22, p = .03; second IC: rho = 0.26, p = .01; third IC: rho = 0.25, p = .01; FWE-corrected for multiple comparisons). Conversely, we did not find any correlation between the logarithmic model evidences of opposed model M_{aR} during aL and opposed model M_{aL} during aR regulation conditions, and the intra-subject trial loadings of the ICs (two-tailed Spearman correlation; all p-values > .17; FWE-corrected for multiple comparisons). We also found a significant correlation between aL and aR loadings for the fifth IC (Fig. S1C, rho = 0.30, p = .04, FWE-corrected for multiple comparisons), which suggests that this IC reflects the carry-over visual-spatial attention between trials of different conditions. Note that spatial-temporal ICs can encompass anticorrelated networks (Beckmann and Smith, 2005): for example, the fifth IC encompasses anticorrelated default-mode and visual-spatial attention networks. We did not find correlations between logarithmic Bayes factors and tensor ICA trial loadings that survived the FWE correction for multiple comparisons (p-values > .3).

Notably, we found that the first and third ICs overlapped significantly with the corresponding GLM contrast maps: namely, the first IC overlapped with the visual perception and visual-spatial attention contrast maps, rho-values = 0.26; and the third IC overlapped with the visual perception contrast map, rho = .43 (Fig. 4D and E).

3.4. Recovery to baseline during rest epochs

To identify brain areas with significant recovery processes, we used whole-brain GLM and a contrast of linear modulation over the 60s rest epoch that was partitioned into three periods of 20s each. We found significant recovery processes in the V1/V2/V3, V1/V2/LG, anterior V3, V5/MT, MCC/SMA, precentral gyrus (PG), precuneus, thalamus, and dlPFC, in the sense that they became less deactivated (Table 3, Fig. 3), which was consistent with the tensor ICA time-series (Figs. 4 and S1).

Using the contrast estimates provided by SPM, we also performed a conjunction analysis between areas that showed gradual recovery and areas that were (de)activated during the regulation and fixation conditions of the neurofeedback runs (Table 3). We found gradual recovery in areas that were deactivated during neurofeedback regulation (V1/V2/V3, V1/V2/LG, V3a, V5/MT and precuneus). To visualize the relative temporal dynamics of the areas that showed a conjunction effect, we illustrated their contrast estimates (Fig. 5). There was no conjunction between areas that showed gradual recovery and areas that were activated during regulation. Despite some minor differences between brain activations and deactivations during aL and aR trials (Fig. 3B and C), there was no difference between recovery processes after aL and aR neurofeedback trials.

For aR regulation trials, post-hoc correlation analysis revealed a significant correlation between the degree of activation and negative gradual recovery during subsequent rest epochs in the bilateral SPL (left SPL rho = .65 and right SPL rho = .68, p = .01, FDR-corrected; Fig. 6A), and between the degree of deactivation and positive gradual recovery during the subsequent rest epochs in the precuneus (rho = 0.62, p = .01, FDR-corrected; Fig. 6B).

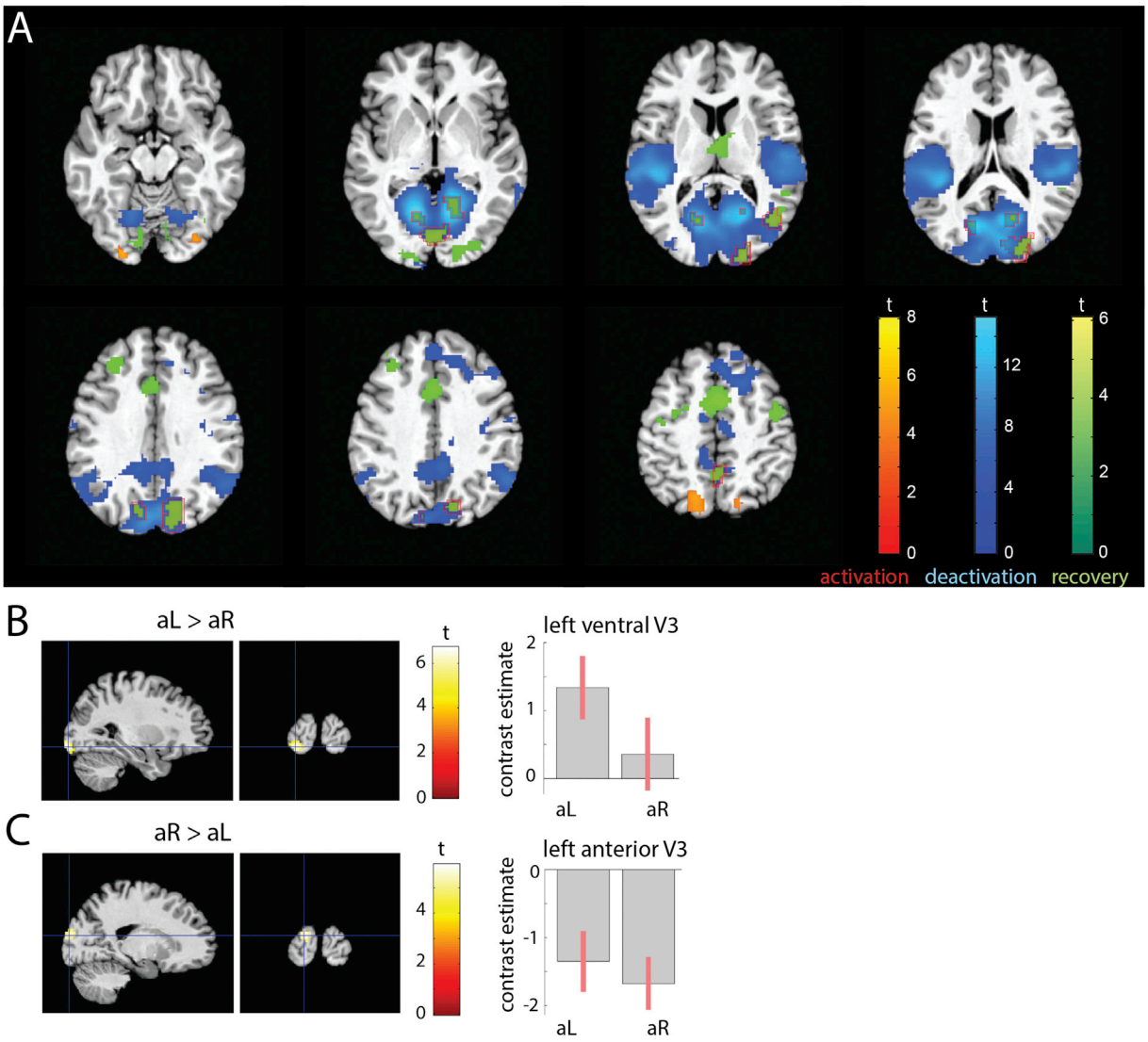

Fig. 3. Covert shifts of visual-spatial attention during neurofeedback regulation and subsequent gradual recovery processes. (A) Neurofeedback regulation through visual-spatial attention shifts to the left (aL) and to the right (aR) were associated with activations (red) in SPL, ventral V3/V4, MFG and IPS, and with deactivations (blue) in the visual cortices V1/V2/V3, LG, V5/MT, IPL, MCC/SMA, SII, precuneus/PCC, medial FC and dlPFC (Table 2). Gradual recovery of brain activity during the rest epochs (green) was found in the MCC/SMA, PG, precuneus, thalamus, dlPFC, and distinct visual cortex regions including V1/V2/V3v, V1/V2/LG, V3a, and V5/MT (Table 3). For illustration, the activation maps were thresholded ($p < .00001$ unc.). ROI contours (red) show the result of conjunction analysis between deactivations during aL and aR trials and the gradual recovery of brain activity during the rest epochs (Table 3). (B) During aL, the left ventral V3 was activated more than during aR. (C) During aR, the left anterior V3 was deactivated more than during aL. (B,C) The right panels display contrast estimates for peak activity and their 90% confidence intervals (red error bars).

3.5. *Mental processes underlying self-regulation*

To control the feedback signal, all but one of the seven participants reported having to covertly shift their visual-spatial attention using visual imagery of activities and movements that overlapped with the displayed dashed circles (Table S2). Our participants reported that control over the neurofeedback signal required a substantial attentional effort (5 ± 0), that successful regulation required utmost concentration (4.6 ± 0.5), that their imagery was highly vivid (4.6 ± 0.8), and that they often included other sensory modalities (2.9 ± 1.8). Interestingly, we found a significant positive correlation between the degree of control over the neurofeedback signal (i.e., neurofeedback success in terms of the logarithmic BF) and the extent of concentration that participants reported ($rho = 0.87$, $p = .03$, Fig. 6C).

4. Discussion

We investigated whether DCM-based neurofeedback and data-driven tensor ICA estimates could be qualitatively linked using data from alternating visual-spatial attention neurofeedback-guided trials. Our results demonstrated correlation between these model-based and data-driven estimates. However, only DCM captured the differences between the alternating visual-spatial attention conditions. These results suggest that data-driven explorative analyses and model-based analyses of neurofeedback studies could complement each other to aid in understanding the target neural network dynamics and regulation mechanisms. In particular, tensor ICA could be used to define the spatiotemporal components constrained to the neurofeedback regulation trials, and aid in the complex connectivity/network definitions through the use of model-based assumptions, such as DCM. These analyses could be performed either prior to the whole-length neurofeedback studies when definition of the target brain area/pattern/network/model is required based on pilot data, or post-hoc to explore the dataset. Systematically investigating the triad of mental effort, spatiotemporal brain network changes, and activity and recovery processes through the

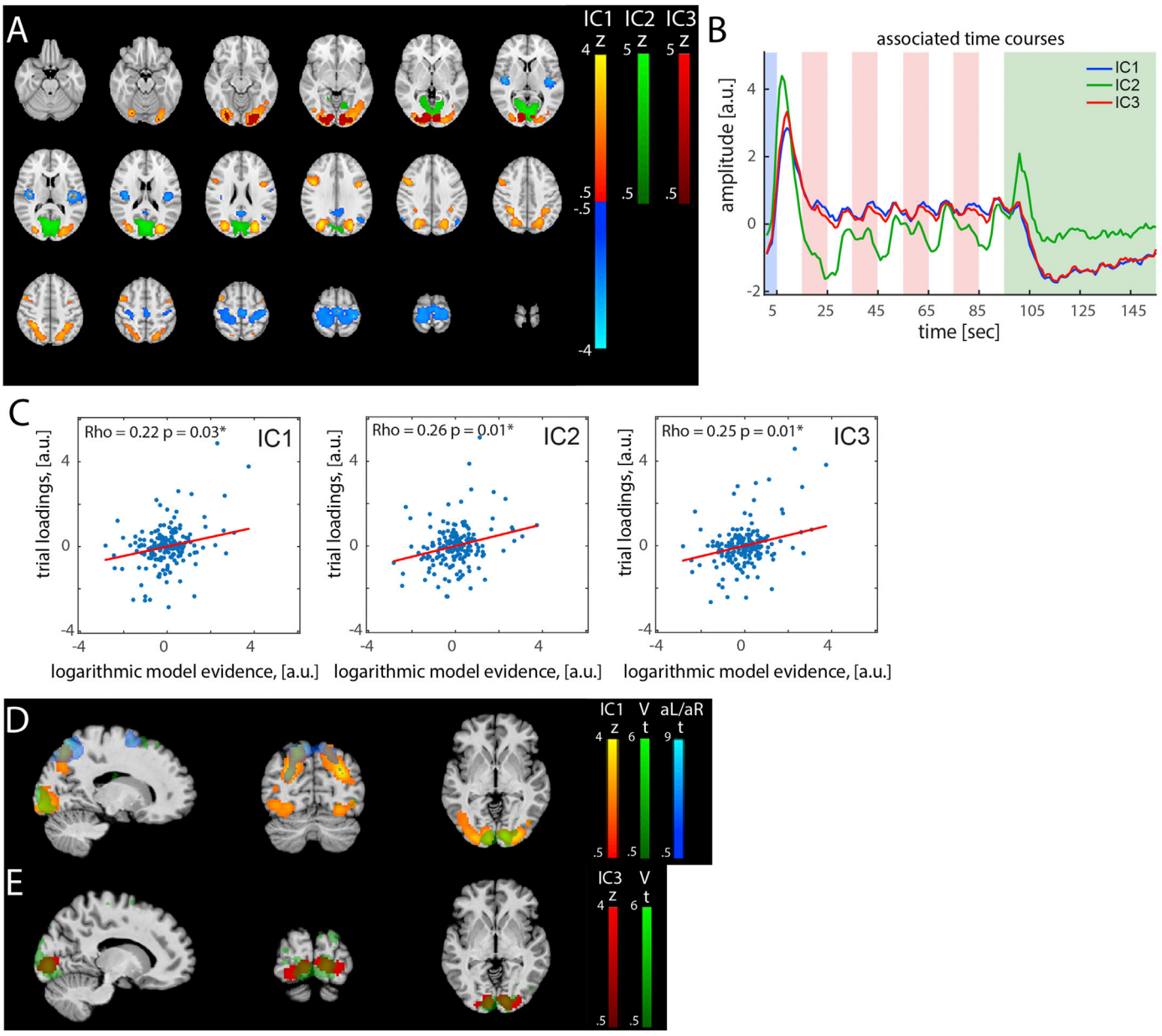

Fig. 4. Linking DCM and ICA for neurofeedback-guided regulation. (A) Thresholded (posterior probability, $p > .5$) first three IC spatial maps, whose intra-subject trial loadings were significantly correlated with the logarithmic model evidences of the target DCM models M_{aL} and M_{aR} during aL and aR trials, respectively. (B) Time-series of the corresponding ICs. (C) Correlation between intra-subject trial loadings and logarithmic model evidences. Asterisks denote statistical significance (FWE-corrected for multiple comparisons, $p < .05$). (D) Spatial overlap between the first IC (orange), visual perception (V, green, rho = .26), and aL/aR (blue, rho = 0.26) contrast maps, and (E) between the third IC (red) and the visual perception (V, green, rho = 0.43) contrast map. For a simplified comparison, we thresholded GLM contrast maps at $p < .01$ unc. as implemented in SPM.

combined use of data-driven and model-based approaches might lead to a better understanding of how learning with neurofeedback is accomplished, and how such learning can cause plastic brain changes along with specific behavioral effects (Harmelech et al., 2013; Megumi et al., 2015; Shibata et al., 2011; Sitaram et al., 2017).

4.1. Controlling the connectivity-based neurofeedback signal

Despite the fact that our study did not target a behavioral outcome, the positive correlation between the extent of concentration and the control over the neurofeedback signal confirmed that successful self-regulation required substantial attention and concentration (Fig. 6). The reported strategies showed that our participants focused mostly on shifting attention to lateralized visual imagery of moving objects and complex scenes (Table S2). This is in line with previous reports showing that, for example, voluntarily modulating the connectivity between the visual and parietal areas by shifting visual-spatial attention requires effort and is associated with visual imagery (Hopfinger et al., 2000).

4.2. Activity changes related to neurofeedback-guided visual-spatial attention

We found that neurofeedback-guided visual-spatial attention regulation resulted in activity changes that were characteristic of the mental strategies used to control the feedback signal. The activity changes

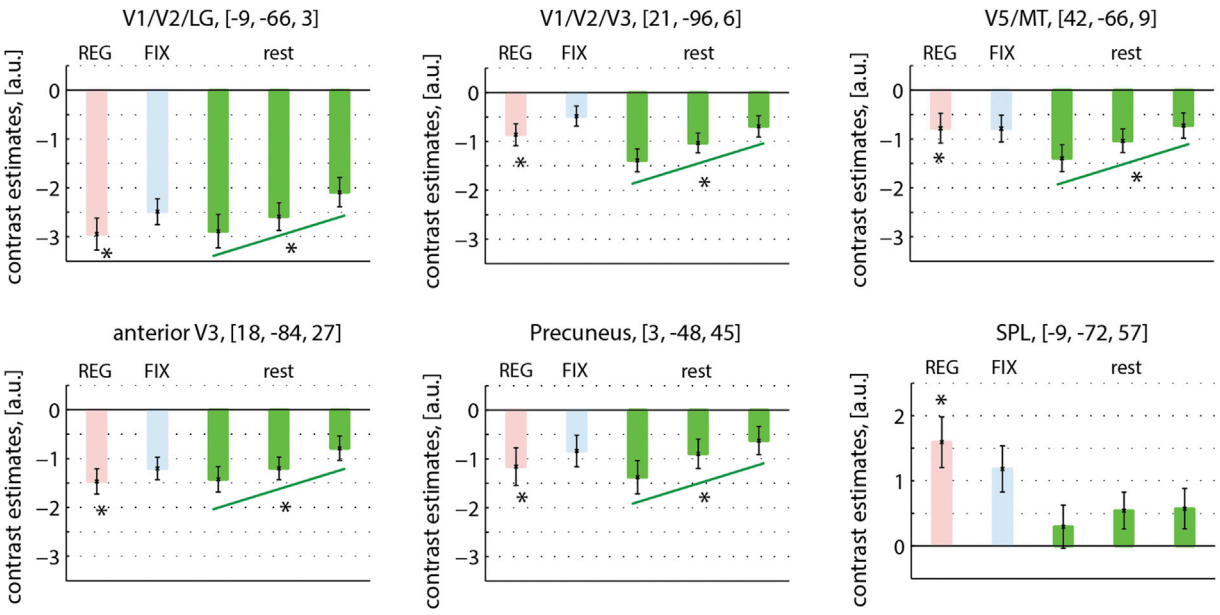

Fig. 5. Displayed are the areas that showed significant conjunction between the contrast estimates for deactivation during neurofeedback regulation (REG) and gradual recovery (Table 3). Red, blue and green blocks denote regulation (REG), fixation with counting (FIX), and rest epochs, respectively. The contrast estimates for the SPL (i.e., an area that did not show a significant gradual recovery process) is shown for comparison. L – left, R – right. Asterisks denote statistical significance (whole-brain FWE, $p < .05$). Vertical bars denote the standard error of the mean.

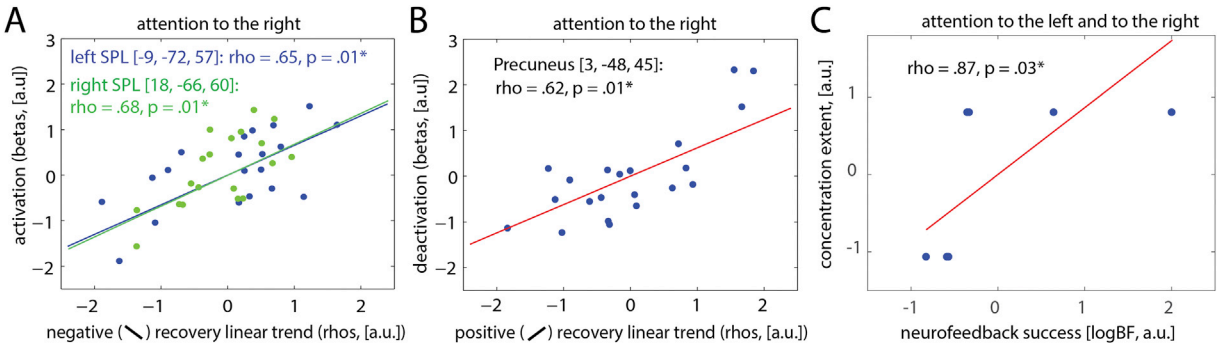

Fig. 6. Correlation between (A) the activation and gradual recovery in the SPL and (B) the deactivation and gradual recovery in the precuneus (separately plotted for each of the 3 trials that every participant performed). For illustration purposes, the negative recovery trend values (panel A, x-axes) and negative beta values of the precuneus deactivations (panel B, y-axes) were inverted, and all the values were z-scored. Notably, these dependencies were observed only for aR conditions. (C) Correlation between the degree of control over the differential neurofeedback signal and the extent of concentration required for successful neurofeedback regulation (plotted for each participant). Asterisks denote statistical significance (FDR-corrected for multiple comparisons, $q < .05$).

during the neurofeedback runs were mainly found in attention-related (SPL) and visual (ventral V3/V4) areas (Fig. 3, Table 2). This is in line with other studies that revealed the role of the parietal cortices in directing covert visual-spatial attention (Greenberg et al., 2010; Hopfinger et al., 2000; Kelley et al., 2008; Yantis et al., 2002). Deactivation is less well characterized in the literature, and typically refers to a decrease of neural activity relative to the baseline level (Amedi et al., 2005; Raichle et al., 2001). During the neurofeedback regulation trials, we found widespread deactivation in the visual cortices, LG, SII, IPL, dlPFC, MCC/SMA, precuneus/PCC, and medial FC (Fig. 3, Table 2). Widespread deactivation in the early visual cortices V1/V2/V3 and LG might be surprising, because covert shifts of attention and visual imagery have often been associated with increased activity in visual areas (Brefczynski and DeYoe, 1999; Guillot et al., 2009; Kastner et al., 1999; Kosslyn et al., 2001; Slotnick et al., 2005; Stokes et al., 2009). However, there are other reports of deactivation in the visual cortices that were associated with imagery (Kaas et al., 2010). Likewise, in another neurofeedback study that involved visual imagery, we also found consistent deactivation in the visual cortex (Scharnowski et al., 2015). We speculate that decreased somatosensory activity during visual imagery might reflect the suppression of concurrent sensory inputs to prevent disruptions of the internally generated mental image (Amedi et al., 2005). The observed deactivation in the bilateral dlPFC, a brain area associated with executive control and maintenance in working memory (Greicius and Menon, 2004; Menon and Uddin, 2010), might reflect the dominance of attention-related tasks over executive control.

The default mode network (DMN) commonly refers to a large-scale cerebral network, and is the hallmark of the resting-state condition (Fox and Raichle, 2007; Laird et al., 2011). It can be defined as the regions that deactivate during experimental tasks when compared to baseline, or, alternatively, using functional-connectivity analysis between brain regions (Amedi et al., 2005; Fox and Raichle, 2007; Greicius et al., 2003). The deactivation in the medial FC, PCC, MCC, and precuneus could be associated with the disengaging DMN during our goal-directed and attention-demanding tasks. For example, parts of the DMN were found to be deactivated during several tasks, including

visual imagery, high attention demands, and working memory (Gusnard et al., 2001; Mayer et al., 2010; Raichle et al., 2001). Quite curiously, we found that using covert shifts of attention to control the neurofeedback signal elicited more widespread (de)activation compared to using the very same strategy during the visual-spatial attention runs without neurofeedback (Figs. 2 and 3; Tables 1 and 2). These qualitative findings reflect other evidence highlighting that the neurofeedback experiment is associated with distinct brain changes (Emmert et al., 2016; Haller et al., 2013; Papageorgiou et al., 2013). However, we cannot infer that observed activity changes are specific to the neurofeedback condition rather than alternated visual-spatial attention regulation in our neurofeedback-guided paradigm, which remains outside the scope of this study and could require a full-length neurofeedback training study and specific control groups (Sitaram et al., 2017).

4.3. Tensor ICA for DCM-based neurofeedback

Hypothesis-driven DCM analysis is a model-based approach that requires solid prior assumptions about the problem being studied, while data-driven ICA is an exploratory data-driven approach that typically requires less prior knowledge (Calhoun and Sui, 2016; Friston, 2011; Friston et al., 2003). In contrast to conventional offline DCM, where one seeks to find the model that best explains the data, DCM-based neurofeedback requires the participants to modulate brain activity (i.e., effective connectivity estimates) such that one of two predefined models dominates the other, thus allowing for training a specific network architecture and causal regulatory mechanisms (Koush et al., 2013, 2015). Nevertheless, for DCM-based neurofeedback, prior assumptions need to be made about the connectivity architecture, including the target and opposed network models, with their ROIs, intrinsic connections, and external and modulatory inputs.

Our results confirmed a qualitative link between the DCM-based and data-driven tensor ICA metrics (Fig. 4A, C), in line with the generally successful use of ICA to define the ROIs for conventional DCM analysis (Di and Biswal, 2014; Li et al., 2012; Sharaev et al., 2016). More specifically, we found that the logarithmic model evidences of target model M_{aL} during aL and target model M_{aR} during aR regulation conditions were correlated with the intra-subject trial loadings of the first three ICs (Fig. 4C, $rho_{first\ IC} = 0.22$, $rho_{second\ IC} = 0.26$, $rho_{third\ IC} = 0.25$), which was not observed for the opposed DCM models. However, we did not find any correlation between the logarithmic Bayes factors and tensor ICA trial loadings. Importantly, SPL and visual cortex areas, which were functionally localized for DCM-based neurofeedback using conventional GLM analysis prior to the neurofeedback runs, largely overlapped with the corresponding ICs (Fig. 4D and E). These findings highlight that DCM metrics in terms of the logarithmic Bayes factor, estimated as the difference between the target and opposed logarithmic model evidences, captured the causal differences between the relatively similar network architectures (Fig. 1; M_{aL} and M_{aR} models with the same ROIs and intrinsic connections, but different external and modulatory inputs), while more generic DCM metrics in terms of the logarithmic target model evidence were consistent with the trial loadings of the ICs. Thus, identifying spatiotemporal ICs might allow for tailoring the target networks to the connectivity-based neurofeedback. Notably, ICs also captured the anticorrelated DMN areas, which was consistent with the whole-brain GLM analysis (Figs. 3 and 5), and emphasized the decreased activity due to the visual imagery and attention tasks as outlined above. Therefore, such analyses could provide insights as to whether the specific regulation mechanism might involve co-(de)activated brain areas or distinct networks such as the DMN. Tensor ICA could aid in the definition of the brain network models and (anti) correlated brain areas/patterns for functional connectivity neurofeedback estimates; for example, it could indicate and limit the number of nodes for complex network models and pair-wise functional (anti)correlations under investigation.

4.4. Gradual recovery following neurofeedback-guided visual-spatial attention

It has been shown that the preceding experimental task might modulate the subsequent resting-state activity (Buckner et al., 2008; Waites et al., 2005), such as in emotional (Eryilmaz et al., 2011), motor (Albert et al., 2009), visual learning (Lewis et al., 2009; Urner et al., 2013), memory (Deuker et al., 2013; Stevens et al., 2010; Tambini et al., 2010) and pain (Riedl et al., 2011) experiments. In line with these findings, resting-state activity has been reported to predict neurofeedback success (Scheinost et al., 2014) and to be modulated by neurofeedback training (Harmelech et al., 2013; Megumi et al., 2015; Ramot et al., 2017; Young et al., 2018; Yuan et al., 2014). We found that induced activity changes were not limited to periods of active self-regulation, but were also evident in distinct gradual recovery processes during the integrated rest epochs. There were two recovery processes that took place (Fig. 4B, Fig. S1B). First, there was a recovery of the deactivated areas during the baseline blocks, which was consistent with a similar recovery process of the DMN activity observed during relatively short (20 s) baseline blocks in a study that trained down-regulation of the primary auditory cortex (Van De Ville et al., 2012). Our results are also in line with previous findings that have demonstrated that resting-state DMN can be modulated through neurofeedback training (Harmelech et al., 2013; Megumi et al., 2015). The second recovery process related to gradual recovery to the baseline level during the relatively long rest epoch after the neurofeedback trial (Fig. 5). We found gradual recovery in areas that showed activity changes during regulation and fixation conditions, namely, the visual cortices (V1/V2/V3, V1/V2/LG, anterior V3, and right V5/MT), MCC/SMA, precuneus, thalamus, and dlPFC (Table 3, Figs. 3 and 5). We also found that areas that exhibited deactivation during neurofeedback spatially overlapped to a large degree with areas that showed a gradual recovery during rest (Table 3, Figs. 3 and 5). Interestingly, recovery in the SPL could be predicted by the level of activation during neurofeedback (Table 3, Fig. 6A), and recovery in the Precuneus could be predicted by the level of deactivation during neurofeedback (Table 3, Fig. 6B). Hence, during rest, activity changes in areas that were associated with the neurofeedback-guided task, notably visual and attention-related areas, gradually recovered to baseline levels. Recovery of the deactivated thalamus, which is the gatekeeper for somatosensory and visual information (McCormick and Bal, 1994), might reflect recovery from the suppression of concurrent sensory inputs that helped to prevent disruptions of the internally generated mental image that was used during neurofeedback-guided trials (Amedi et al., 2005). Recovery of DMN-related deactivation likely reflected task-disengagement after neurofeedback regulation, which required participants to concentrate and exert vivid visual imagery (Fig. 6**C**). This is well in line with previous findings showing that fast performance in a selective-attention task (Weissman et al., 2006), and in a psychomotor vigilance task (Thompson et al., 2013), was associated with higher anticorrelation between task-related activation and DMN deactivation. In addition, Weissman et al. have shown that early attentional lapses were characterized by less efficient stimulus processing, by less deactivation in the DMN, and by less stimulus-evoked sensory activity. Finally, the time-series of the first, third, and fifth to seventh ICs highlighted the striking similarity with the recovery processes identified with whole-brain GLM analysis (compare Figs. 4B and S1B and Fig. 5).

4.5. Specificity of the DCM-based neurofeedback

Despite having identified some lateralization in the visual cortices specific to the left and right attention shift using whole-brain GLM (Fig. 3B and C), we did not find any differences in aL and aR neurofeedback-guided regulation and recovery after regulation, and between the aL and aR tensor ICA trial loadings. The correlation between aL and aR loadings for the fifth IC might indicate that this IC reflected a general brain state of attention (i.e., the spatial map shows default-mode

vs. visual-spatial attention networks) that carried over between trials of different conditions, while the loadings of the other ICs captured within-trial effects. Therefore, in general, the differences between the aL and aR neurofeedback trials were captured exclusively by the DCM estimates (i.e., by increased target model exceedance probabilities $Pe_{MaL} = 0.86$ and $Pe_{MaR} = 0.77$, respectively) given the same areas involved in aL and aR regulation tasks (Fig. 1) (Koush et al., 2013). These findings further highlight the specificity of the causal DCM-based neurofeedback estimates, which captured specific network interdependencies and regulation mechanisms that could not otherwise be revealed by whole-brain GLM or tensor ICA analyses.

Acknowledgements

This study was supported in part by the Swiss National Science Foundation (YK: P300PB_161083; FS: BSSG10_155915, 32003B_166566, 100014_178841) and in part by a Pilot Grant of the Wyss Center at the Campus Biotech Geneva. FS is also supported by the Foundation for Research in Science and the Humanities at the University of Zurich (STWF-17-012) and by the Baugarten Stiftung. The authors declare no competing financial interests.

Appendix A. Supplementary data

Supplementary data related to this article can be found at https://doi.org/10.1016/j.neuroimage.2018.08.067.

References

Albert, N.B., Robertson, E.M., Miall, R.C., 2009. The resting human brain and motor learning. Curr. Biol. 19, 1023–1027.
Amano, K., Shibata, K., Kawato, M., Sasaki, Y., Watanabe, T., 2016. Learning to associate orientation with color in early visual areas by associative decoded fMRI neurofeedback. Curr. Biol. 26, 1861–1866.
Amedi, A., Malach, R., Pascual-Leone, A., 2005. Negative BOLD differentiates visual imagery and perception. Neuron 48, 859–872.
Ashburner, J., 2007. A fast diffeomorphic image registration algorithm. Neuroimage 38, 95–113.
Bassett, D.S., Sporns, O., 2017. Network neuroscience. Nat. Neurosci. 20, 353–364.
Beckmann, C.F., 2012. Modelling with independent components. Neuroimage 62, 891–901.
Beckmann, C.F., Noble, J.A., Smith, S.M., 2001. Investigating the intrinsic dimensionality of FMRI data for ICA. Neuroimage 13. S76-S76.
Beckmann, C.F., Smith, S.A., 2004. Probabilistic independent component analysis for functional magnetic resonance imaging. IEEE Trans. Med. Imag. 23, 137–152.
Beckmann, C.F., Smith, S.M., 2005. Tensorial extensions of independent component analysis for multisubject FMRI analysis. Neuroimage 25, 294–311.
Blankenburg, F., Ruff, C.C., Bestmann, S., Bjoertomt, O., Josephs, O., Deichmann, R., Driver, J., 2010. Studying the role of human parietal cortex in visuospatial attention with concurrent TMS-fMRI. Cerebr. Cortex 20, 2702–2711.
Braun, U., Schaefer, A., Betzel, R.F., Tost, H., Meyer-Lindenberg, A., Bassett, D.S., 2018. From maps to multi-dimensional network mechanisms of mental disorders. Neuron 97, 14–31.
Brefczynski, J.A., DeYoe, E.A., 1999. A physiological correlate of the 'spotlight' of visual attention. Nat. Neurosci. 2, 370–374.
Bressler, S.L., Tang, W., Sylvester, C.M., Shulman, G.L., Corbetta, M., 2008a. Top-down control of human visual cortex by frontal and parietal cortex in anticipatory visual spatial attention. J. Neurosci. 28, 10056–10061.
Bressler, S.L., Tang, W., Sylvester, C.M., Shulman, G.L., Corbetta, M., 2008b. Top-down control of human visual cortex by frontal and parietal cortex in anticipatory visual spatial attention. J. Neurosci. 28, 10056–10061.
Buckner, R.L., Andrews-Hanna, J.R., Schacter, D.L., 2008. The brain's default network: anatomy, function, and relevance to disease. Ann. N. Y. Acad. Sci. 1124, 1–38.
Calhoun, V.D., Sui, J., 2016. Multimodal fusion of brain imaging data: a key to finding the missing link(s) in complex mental illness. Biol Psychiatry Cogn Neurosci Neuroimaging 1, 230–244.
deBettencourt, M.T., Cohen, J.D., Lee, R.F., Norman, K.A., Turk-Browne, N.B., 2015. Closed-loop training of attention with real-time brain imaging. Nat. Neurosci. 18, 470–475.
deCharms, R.C., 2008. Applications of real-time fMRI. Nat. Rev. Neurosci. 9, 720–729.
Deuker, L., Olligs, J., Fell, J., Kranz, T.A., Mormann, F., Montag, C., Reuter, M., Elger, C.E., Axmacher, N., 2013. Memory consolidation by replay of stimulus-specific neural activity. J. Neurosci. 33, 19373–19383.
Di, X., Biswal, B.B., 2014. Identifying the default mode network structure using dynamic causal modeling on resting-state functional magnetic resonance imaging. Neuroimage 86, 53–59.
Eickhoff, S.B., Stephan, K.E., Mohlberg, H., Grefkes, C., Fink, G.R., Amunts, K., Zilles, K., 2005. A new SPM toolbox for combining probabilistic cytoarchitectonic maps and functional imaging data. Neuroimage 25, 1325–1335.
Emmert, K., Kopel, R., Sulzer, J., Bruhl, A.B., Berman, B.D., Linden, D.E.J., Horovitz, S.G., Breimhorst, M., Caria, A., Frank, S., Johnston, S., Long, Z., Paret, C., Robineau, F., Veit, R., Bartsch, A., Beckmann, C.F., Van De Ville, D., Haller, S., 2016. Meta-analysis of real-time fMRI neurofeedback studies using individual participant data: how is brain regulation mediated? Neuroimage 124, 806–812.
Eryilmaz, H., Van De Ville, D., Schwartz, S., Vuilleumier, P., 2011. Impact of transient emotions on functional connectivity during subsequent resting state: a wavelet correlation approach. Neuroimage 54, 2481–2491.
Esposito, F., Seifritz, E., Formisano, E., Morrone, R., Scarabino, T., Tedeschi, G., Cirillo, S., Goebel, R., Di Salle, F., 2003. Real-time independent component analysis of fMRI time-series. Neuroimage 20, 2209–2224.
Fox, M.D., Raichle, M.E., 2007. Spontaneous fluctuations in brain activity observed with functional magnetic resonance imaging. Nat. Rev. Neurosci. 8, 700–711.
Friston, K., Phillips, J., Chawla, D., Buchel, C., 1999. Revealing interactions among brain systems with nonlinear PCA. Hum. Brain Mapp. 8, 92–97.
Friston, K.J., 2011. Functional and effective connectivity: a review. Brain Connect. 1, 13–36.
Friston, K.J., Harrison, L., Penny, W., 2003. Dynamic causal modelling. Neuroimage 19, 1273–1302.
Greenberg, A.S., Esterman, M., Wilson, D., Serences, J.T., Yantis, S., 2010. Control of spatial and feature-based attention in frontoparietal cortex. J. Neurosci.: the official journal of the Society for Neuroscience 30, 14330–14339.
Greicius, M.D., Krasnow, B., Reiss, A.L., Menon, V., 2003. Functional connectivity in the resting brain: a network analysis of the default mode hypothesis. Proc. Natl. Acad. Sci. U. S. A. 100, 253–258.
Greicius, M.D., Menon, V., 2004. Default-mode activity during a passive sensory task: uncoupled from deactivation but impacting activation. J. Cognit. Neurosci. 16, 1484–1492.
Guillot, A., Collet, C., Nguyen, V.A., Malouin, F., Richards, C., Doyon, J., 2009. Brain activity during visual versus kinesthetic imagery: an fMRI study. Hum. Brain Mapp. 30, 2157–2172.
Gusnard, D.A., Akbudak, E., Shulman, G.L., Raichle, M.E., 2001. Medial prefrontal cortex and self-referential mental activity: relation to a default mode of brain function. Proc. Natl. Acad. Sci. U. S. A. 98, 4259–4264.
Haller, S., Kopel, R., Jhooti, P., Haas, T., Scharnowski, F., Lovblad, K.-O., Scheffler, K., Van De Ville, D., 2013. Dynamic reconfiguration of human brain functional networks through neurofeedback. Neuroimage 81, 243–252.
Harmelech, T., Preminger, S., Wertman, E., Malach, R., 2013. The day-after effect: long term, Hebbian-like restructuring of resting-state fMRI patterns induced by a single epoch of cortical activation. J. Neurosci. 33, 9488–9497.
Hopfinger, J.B., Buonocore, M.H., Mangun, G.R., 2000. The neural mechanisms of top-down attentional control. Nat. Neurosci. 3, 284–291.
Hoyer, P.O., 2004. Non-negative matrix factorization with sparseness constraints. J. Mach. Learn. Res. 5, 1457–1469.
Kaas, A., Weigelt, S., Roebroeck, A., Kohler, A., Muckli, L., 2010. Imagery of a moving object: the role of occipital cortex and human MT/V5+. Neuroimage 49, 794–804.
Kajal, D.S., Braun, C., Mellinger, J., Sacchet, M.D., Ruiz, S., Fetz, E., Birbaumer, N., Sitaram, R., 2017. Learned control of inter-hemispheric connectivity: effects on bimanual motor performance. Hum. Brain Mapp. 38, 4353–4369.
Kastner, S., Pinsk, M.A., De Weerd, P., Desimone, R., Ungerleider, L.G., 1999. Increased activity in human visual cortex during directed attention in the absence of visual stimulation. Neuron 22, 751–761.
Kelley, T.A., Serences, J.T., Giesbrecht, B., Yantis, S., 2008. Cortical mechanisms for shifting and holding visuospatial attention. Cerebr. Cortex 18, 114–125.
Kelly Jr., R.E., Alexopoulos, G.S., Wang, Z., Gunning, F.M., Murphy, C.F., Morimoto, S.S., Kanellopoulos, D., Jia, Z., Lim, K.O., Hoptman, M.J., 2010. Visual inspection of independent components: defining a procedure for artifact removal from fMRI data. J. Neurosci. Meth. 189, 233–245.
Kim, D.Y., Yoo, S.S., Tegethoff, M., Meinlschmidt, G., Lee, J.H., 2015. The inclusion of functional connectivity information into fMRI-based neurofeedback improves its efficacy in the reduction of cigarette cravings. J. Cognit. Neurosci. 27, 1552–1572.
Kosslyn, S.M., Ganis, G., Thompson, W.L., 2001. Neural foundations of imagery. Nat. Rev. Neurosci. 2, 635–642.
Koush, Y., Ashburner, J., Prilepin, E., Sladky, R., Zeidman, P., Bibikov, S., Scharnowski, F., Nikonorov, A., De Ville, D.V., 2017a. OpenNFT: an open-source Python/Matlab framework for real-time fMRI neurofeedback training based on activity, connectivity and multivariate pattern analysis. Neuroimage 156, 489–503.
Koush, Y., Ashburner, J., Prilepin, E., Sladky, R., Zeidman, P., Bibikov, S., Scharnowski, F., Nikonorov, A., Van De Ville, D., 2017b. Real-time fMRI data for testing OpenNFT functionality. Data Brief 14, 344–347.
Koush, Y., Meskaldji, D.E., Pichon, S., Rey, G., Rieger, S.W., Linden, D.E., Van De Ville, D., Vuilleumier, P., Scharnowski, F., 2015. Learning control over emotion networks through connectivity-based neurofeedback. Cerebr. Cortex.
Koush, Y., Rosa, M.J., Robineau, F., Heinen, K., S, W.R., Weiskopf, N., Vuilleumier, P., Van De Ville, D., Scharnowski, F., 2013. Connectivity-based neurofeedback: dynamic causal modeling for real-time fMRI. Neuroimage 81, 422–430.
Koush, Y., Zvyagintsev, M., Dyck, M., Mathiak, K.A., Mathiak, K., 2012. Signal quality and Bayesian signal processing in neurofeedback based on real-time fMRI. Neuroimage 59, 478–489.
LaConte, S.M., 2011. Decoding fMRI brain states in real-time. Neuroimage 56, 440–454.
LaConte, S.M., Peltier, S.J., Hu, X.P.P., 2007. Real-time fMRI using brain-state classification. Hum. Brain Mapp. 28, 1033–1044.

Laird, A.R., Fox, P.M., Eickhoff, S.B., Turner, J.A., Ray, K.L., McKay, D.R., Glahn, D.C., Beckmann, C.F., Smith, S.M., Fox, P.T., 2011. Behavioral interpretations of intrinsic connectivity networks. J. Cognit. Neurosci. 23, 4022–4037.
Lewis, C.M., Baldassarre, A., Committeri, G., Romani, G.L., Corbetta, M., 2009. Learning sculpts the spontaneous activity of the resting human brain. Proc. Natl. Acad. Sci. U. S. A. 106, 17558–17563.
Li, B.J., Wang, X., Yao, S.Q., Hu, D.W., Friston, K.J., 2012. Task-dependent modulation of effective connectivity within the default mode network. Front. Psychol. 3.
Liew, S.L., Rana, M., Cornelsen, S., Fortunato de Barros Filho, M., Birbaumer, N., Sitaram, R., Cohen, L.G., Soekadar, S.R., 2016. Improving motor corticothalamic communication after stroke using real-time fMRI connectivity-based neurofeedback. Neurorehabilitation Neural Repair 30, 671–675.
Lohmann, G., Volz, K.G., Ullsperger, M., 2007. Using non-negative matrix factorization for single-trial analysis of fMRI data. Neuroimage 37, 1148–1160.
Mayer, J.S., Roebroeck, A., Maurer, K., Linden, D.E.J., 2010. Specialization in the default mode: task-induced brain deactivations dissociate between visual working memory and attention. Hum. Brain Mapp. 31, 126–139.
McCormick, D.A., Bal, T., 1994. Sensory gating mechanisms of the thalamus. Curr. Opin. Neurobiol. 4, 550–556.
Megumi, F., Yamashita, A., Kawato, M., Imamizu, H., 2015. Functional MRI neurofeedback training on connectivity between two regions induces long-lasting changes in intrinsic functional network. Front. Hum. Neurosci. 9, 160.
Menon, V., Uddin, L.Q., 2010. Saliency, switching, attention and control: a network model of insula function. Brain Struct. Funct. 214, 655–667.
Minka, T., 2000. Automatic Choice of Dimensionality for PCA. MIT Media Lab Vision and Modeling Group. Technical Report 514.
Papageorgiou, T.D., Lisinski, J.M., McHenry, M.A., White, J.P., LaConte, S.M., 2013. Brain-computer interfaces increase whole-brain signal to noise. Proc. Natl. Acad. Sci. U. S. A. 110, 13630–13635.
Raichle, M.E., MacLeod, A.M., Snyder, A.Z., Powers, W.J., Gusnard, D.A., Shulman, G.L., 2001. A default mode of brain function. Proc. Natl. Acad. Sci. U. S. A. 98, 676–682.
Ramot, M., Kimmich, S., Gonzalez-Castillo, J., Roopchansingh, V., Popal, H., White, E., Gotts, S.J., Martin, A., 2017. Direct modulation of aberrant brain network connectivity through real-time NeuroFeedback. Elife 6.
Riedl, V., Valet, M., Woller, A., Sorg, C., Vogel, D., Sprenger, T., Boecker, H., Wohlschlager, A.M., Tolle, T.R., 2011. Repeated pain induces adaptations of intrinsic brain activity to reflect past and predict future pain. Neuroimage 57, 206–213.
Scharnowski, F., Veit, R., Zopf, R., Studer, P., Bock, S., Diedrichsen, J., Goebel, R., Mathiak, K., Birbaumer, N., Weiskopf, N., 2015. Manipulating motor performance and memory through real-time fMRI neurofeedback. Biol. Psychol. 108, 85–97.
Scheinost, D., Stoica, T., Wasylink, S., Gruner, P., Saksa, J., Pittenger, C., Hampson, M., 2014. Resting state functional connectivity predicts neurofeedback response. Front. Behav. Neurosci. 8, 338.
Sharaev, M.G., Zavyalova, V.V., Ushakov, V.L., Kartashov, S.I., Velichkovsky, B.M., 2016. Effective connectivity within the default mode network: dynamic causal modeling of resting-state fMRI data. Front. Hum. Neurosci. 10, 14.
Shibata, K., Watanabe, T., Sasaki, Y., Kawato, M., 2011. Perceptual learning incepted by decoded fMRI neurofeedback without stimulus presentation. Science 334, 1413–1415.
Sitaram, R., Ros, T., Stoeckel, L., Haller, S., Scharnowski, F., Lewis-Peacock, J., Weiskopf, N., Blefari, M.L., Rana, M., Oblak, E., Birbaumer, N., Sulzer, J., 2017. Closed-loop brain training: the science of neurofeedback. Nature Neuroscience Reviews.
Slotnick, S.D., Thompson, W.L., Kosslyn, S.M., 2005. Visual mental imagery induces retinotopically organized activation of early visual areas. Cerebr. Cortex 15, 1570–1583.
Smith, S.M., Fox, P.T., Miller, K.L., Glahn, D.C., Fox, P.M., Mackay, C.E., Filippini, N., Watkins, K.E., Toro, R., Laird, A.R., Beckmann, C.F., 2009. Correspondence of the brain's functional architecture during activation and rest. Proc. Natl. Acad. Sci. U. S. A. 106, 13040–13045.
Soldati, N., Calhoun, V.D., Bruzzone, L., Jovicich, J., 2013. ICA analysis of fMRI with real-time constraints: an evaluation of fast detection performance as function of algorithms, parameters and a priori conditions. Front. Hum. Neurosci. 7, 19.
Stephan, K.E., Penny, W.D., Daunizeau, J., Moran, R.J., Friston, K.J., 2009. Bayesian model selection for group studies. Neuroimage 46, 1004–1017.
Stevens, W.D., Buckner, R.L., Schacter, D.L., 2010. Correlated low-frequency BOLD fluctuations in the resting human brain are modulated by recent experience in category-preferential visual regions. Cerebr. Cortex 20, 1997–2006.
Stokes, M., Thompson, R., Cusack, R., Duncan, J., 2009. Top-down activation of shape-specific population codes in visual cortex during mental imagery. J. Neurosci. 29, 1565–1572.
Sulzer, J., Haller, S., Scharnowski, F., Weiskopf, N., Birbaumer, N., Blefari, M.L., Bruehl, A.B., Cohen, L.G., DeCharms, R.C., Gassert, R., Goebel, R., Herwig, U., LaConte, S., Linden, D., Luft, A., Seifritz, E., Sitaram, R., 2013. Real-time fMRI neurofeedback: progress and challenges. Neuroimage 76, 386–399.
Tambini, A., Ketz, N., Davachi, L., 2010. Enhanced brain correlations during rest are related to memory for recent experiences. Neuron 65, 280–290.
Thompson, G.J., Magnuson, M.E., Merritt, M.D., Schwarb, H., Pan, W.-J., McKinley, A., Tripp, L.D., Schumacher, E.H., Keilholz, S.D., 2013. Short-time windows of correlation between large-scale functional brain networks predict vigilance intraindividually and interindividually. Hum. Brain Mapp. 34, 3280–3298.
Urner, M., Schwarzkopf, D.S., Friston, K., Rees, G., 2013. Early visual learning induces long-lasting connectivity changes during rest in the human brain. Neuroimage 77, 148–156.
Van De Ville, D., Jhooti, P., Haas, T., Kopel, R., Lovblad, K.O., Scheffler, K., Haller, S., 2012. Recovery of the default mode network after demanding neurofeedback training occurs in spatio-temporally segregated subnetworks. Neuroimage 63, 1775–1781.
Waites, A.B., Stanislavsky, A., Abbott, D.F., Jackson, G.D., 2005. Effect of prior cognitive state on resting state networks measured with functional connectivity. Hum. Brain Mapp. 24, 59–68.
Weissman, D.H., Roberts, K.C., Visscher, K.M., Woldorff, M.G., 2006. The neural bases of momentary lapses in attention. Nat. Neurosci. 9, 971–978.
Worsley, K.J., Poline, J.B., Friston, K.J., Evans, A.C., 1997. Characterizing the response of PET and fMRI data using multivariate linear models. Neuroimage 6, 305–319.
Yamashita, A., Hayasaka, S., Kawato, M., Imamizu, H., 2017. Connectivity neurofeedback training can differentially change functional connectivity and cognitive performance. Cerebr. Cortex 27, 4960–4970.
Yantis, S., Schwarzbach, J., Serences, J.T., Carlson, R.L., Steinmetz, M.A., Pekar, J.J., Courtney, S.M., 2002. Transient neural activity in human parietal cortex during spatial attention shifts. Nat. Neurosci. 5, 995–1002.
Young, K.D., Siegle, G.J., Misaki, M., Zotev, V., Phillips, R., Drevets, W.C., Bodurka, J., 2018. Altered task-based and resting-state amygdala functional connectivity following real-time fMRI amygdala neurofeedback training in major depressive disorder. Neuroimage Clin 17, 691–703.
Yuan, H., Young, K.D., Phillips, R., Zotev, V., Misaki, M., Bodurka, J., 2014. Resting-state functional connectivity modulation and sustained changes after real-time functional magnetic resonance imaging neurofeedback training in depression. Brain Connect. 4, 690–701.
Zilverstand, A., Sorger, B., Zimmermann, J., Kaas, A., Goebel, R., 2014. Windowed correlation: a suitable tool for providing dynamic fMRI-based functional connectivity neurofeedback on task difficulty. PLoS One 9, e85929.